JOURNAL OF Materials CHEMISTRY

Synthesis, stability and zeolitic behavior of δ-ALn_3F_{10},xH_2O and γ-$ThLn_2F_{10},H_2O$ phases (Ln = lanthanide)

Francoise Le Berre, Eric Boucher, Magali Allain and Georges Courbion*

Laboratoire des Fluorures (UPRES A 6010, CNRS), Faculté des Sciences de Mans, Université du Maine, Avenue Olivier Messiaen, 72085 Le Mans Cedex 9, France. E-mail: Georges.Courbion@univ-lemans.fr

Received 30th March 2000, Accepted 26th June 2000
First published as an Advance Article on the web 18th September 2000

Two series of hydrated fluorides have been prepared by a "chimie douce" process. For the first family, more than twenty five compounds of δ-ALn_3F_{10},xH_2O (A^+ = alkaline ions, NH_4^+, H_3O^+ and Ln = lanthanide) have been prepared. They crystallize in the $Fd\bar{3}m$ space group ($a \approx 15.4$ Å and $Z = 16$) and are isotypic with δ-$(H_3O)Yb_3F_{10},xH_2O$ ($x = 1$). The diamond-type structure of these phases (diamond stacking of octahedral units of antiprisms, called $UOA_{[8]}$), creates cavities and tunnels where the water molecules can move.

The second family, γ-$ThLn_2F_{10},H_2O$ ($Ln^{3+} = Er^{3+}$, Dy^{3+} and Yb^{3+}) results from the substitution of Ln^{3+} and A^+ by a tetravalent cation. The new compound γ-$ThEr_2F_{10},H_2O$ ($Fm\bar{3}m$ space group, $a = 10.739(1)$ Å and $Z = 8$) is isotypic with γ-KYb_3F_{10}. Water molecules are located inside the tunnels (8c sites) of a CCP stacking of $UOA_{[8]}$ through which they can move.

For both series, the thermal stability and the zeolitic behaviour, studied by DTA/TGA and X-ray thermodiffractometry, are reported and a low zeolitic water capacity, around 2–4% in mass, is observed.

Introduction

Numerous fluoride compounds involving lanthanide elements and alkaline metals or alkaline earth metals are known. Among them, we found different structural types corresponding to the formula ALn_3F_{10} (Ln = lanthanide). The study of the KF–YbF_3 system led to the discovery of three polymorphs.[1] The first one, α-KYb_3F_{10}, encountered at low temperature, crystallizes in the $Fm\bar{3}m$ space group with $a = 11.431(6)$ Å ($Z = 8$). On heating, this phase gives rise to a β hexagonal form at $T = 769\,^{\circ}C$.[2] This non-reversible transition (not observable by DTA) has been determined by electrical conductivity measurements.[1] For $T = 952\,^{\circ}C$, a reversible transition is observed leading to a γ variety, isotypic to the low temperature form α-KYb_3F_{10}. Starting from these phases, and especially from γ-KYb_3F_{10}, numerous isotypic compounds have been synthesized involving different alkaline cations and rare earth ions.[3,4] A common fact between all these phases, is that they cannot be synthesized with all the lanthanides series.

Recently, a new fluorinated phase $(H_3O)Yb_3F_{10},xH_2O$ has been discovered in the laboratory.[5] It is synthesized at low temperature by a "chimie douce" process and crystallizes in the $Fd\bar{3}m$ space group with $a = 15.326(1)$ Å and $Z = 16$. After several trials, the isotypic KYb_3F_{10},xH_2O phase was obtained. Referring to the different KYb_3F_{10} types known, this new member of the KYb_3F_{10} family has been named δ-KYb_3F_{10},xH_2O. Its structure is based on the association of YbF_8 square antiprisms whose particular arrangement creates cavities and tunnels where water molecules are mobile, thus conferring a zeolitic character.

In order to fully characterize this new zeolitic δ-ALn_3F_{10},xH_2O family, cationic substitutions concerning the alkaline metal and the lanthanide have been performed ($A^+ = H_3O^+$, Li^+, Na^+, K^+, Rb^+, Cs^+, NH_4^+; $Ln^{3+} = Ho^{3+}$, Er^{3+}, Tm^{3+}, Yb^{3+}, Lu^{3+} and Y^{3+}). Furthermore, in the search for more open networks, we found a new cubic zeolitic phase, γ-$ThLn_2F_{10},H_2O$ whose characterisation is also presented.

This paper is divided into two parts, the first concerns the series δ-ALn_3F_{10},xH_2O and the second deals with the γ-$ThLn_2F_{10},H_2O$ family.

A δ-ALn_3F_{10},xH_2O series

1 Synthesis

Contrary to all the anhydrous compounds described above which were synthesized at high temperature, the δ-ALn_3F_{10},xH_2O phases were obtained by a "chimie douce" route. Except for $A^+ = Li^+$ or Na^+, the compounds were directly obtained by addition of a hydrated oxalate $Ln_2(C_2O_4)_3,xH_2O$ (0.7 g) to a heated solution of HF (20 ml of HF 40%) and AF in excess ([AF]/[Ln] = 0.9). After filtration, washing with distilled water and air drying, fine white or pale coloured powders were collected.

This process allowed the synthesis of δ-ALn_3F_{10},xH_2O phases with $A^+ = H_3O^+$, K^+, Rb^+, NH_4^+ and Cs^+ and with small rare earth ($Ln^{3+} = Er^{3+}$, Tm^{3+}, Yb^{3+}, Lu^{3+}) and Y^{3+}. All trials with bigger rare earth cations yielded LnF_3, except for $A^+ = K^+$ in the case of holmium (δ-KHo_3F_{10},xH_2O). With $A^+ = K^+$, particular attention must be focused on the ratio. Indeed, this ratio must be inferior to a given value in order to avoid α-KLn_3F_{10} phase formation; this value depends on the nature of the lanthanide (Fig. 1).

The maximum temperature which yields the best phase crystallinity was found to be a function only of the rare earth's

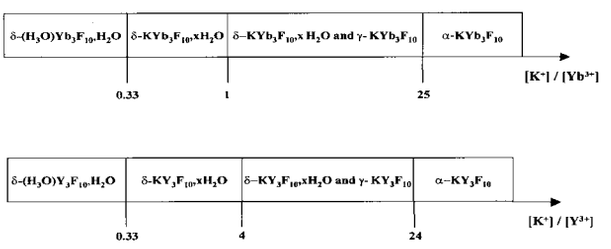

Fig. 1 Existing phases as a function of the $[K^+]/[Ln^{3+}]$ ratio for δ-KY_3F_{10},xH_2O and δ-KYb_3F_{10},xH_2O.

 DOI: 10.1039/b002520h

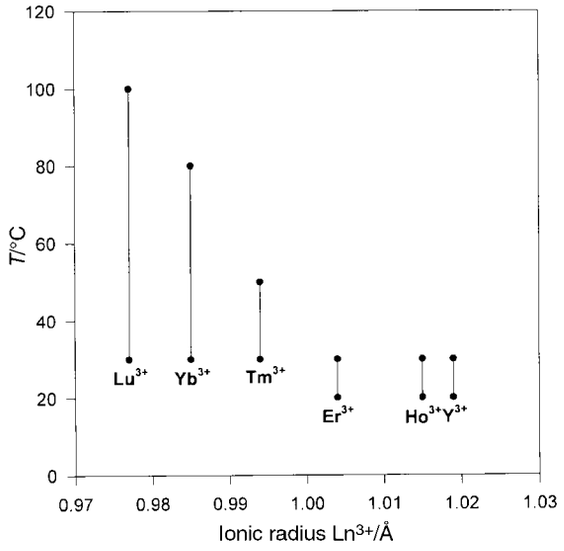

Fig. 2 Synthesis temperature of δ-ALn_3F_{10},xH_2O as a function of the rare earth ionic radii.

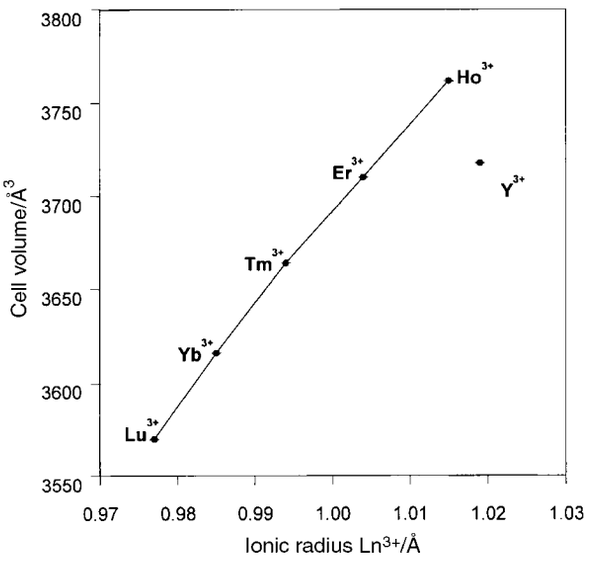

Fig. 3 Cell parameters *versus* rare earth ionic radii for δ-KLn_3F_{10},xH_2O.

size and not of the nature of the A^+ ion. Indeed, as we can see from Fig. 2, the bigger the ionic radius of the rare earth, the lower is the maximum synthesis temperature. For $Ln^{3+}=Er^{3+}$, which is the biggest lanthanide we could use, the temperature is approximatively 30 °C and a lower temperature leads to an amorphous compound.

Concerning the phase δ-ALn_3F_{10},xH_2O with smaller counter-ions A^+ such as Li^+ or Na^+, all our attempts using the synthesis described above were unsuccessful. These phases can only be obtained from δ-$(H_3O)Ln_3F_{10},xH_2O$ by cationic exchange in aqueous solutions containing Li^+ or Na^+. The exchange was carried out by treating 0.2 g of the parent phase in 15 ml of 2 M $LiNO_3$ (or $NaNO_3$) with constant stirring over one hour. The exchange must be performed at the synthesis temperature of the starting compound; for lower temperatures, the exchange ratio doesn't reach its upper value, and for higher temperatures, the phase begins to decompose. Moreover, several cycles are necessary to optimise the exchange. Using δ-$(H_3O)Ln_3F_{10},xH_2O$ as the parent phase, only compounds with Y^{3+} and $Ln^{3+}=Er^{3+}$, Tm^{3+}, Yb^{3+}, Lu^{3+} have been obtained.

We note that the δ-$(NH_4)Ln_3F_{10},xH_2O$ phases can also be prepared by acid–base reaction: the starting compound δ-$(H_3O)Ln_3F_{10},xH_2O$ is placed in a dessicator in the presence of ammonia solution. After several days in this atmosphere, the reaction is complete and leads to the δ-$(NH_4)Ln_3F_{10},xH_2O$ phase.

All the obtained compounds are listed in Table 1.

Table 1 Thermal characteristics and cell parameters of the δ-ALn_3F_{10},xH_2O compounds

Compounds	Color	a/Å	T_1[a]/°C	T_2[b]/°C
δ-$(H_3O)Lu_3F_{10},xH_2O$	White	15.2948(10)	140	310
δ-$(H_3O)Yb_3F_{10},xH_2O$	White	15.3448(7)	144	290
δ-$(H_3O)Tm_3F_{10},xH_2O$	White	15.4314(11)	149	263
δ-$(H_3O)Er_3F_{10},xH_2O$	Pale rose	15.5001(15)	153	268
δ-$(H_3O)Y_3F_{10},xH_2O$	White	15.5112(9)	124	258
δ-KLu_3F_{10},xH_2O	White	15.2830(11)	152	454[c]
δ-KYb_3F_{10},xH_2O	White	15.3484(7)	168	433[c]
δ-KTm_3F_{10},xH_2O	White	15.4164(9)	170	427[c]
δ-KEr_3F_{10},xH_2O	Pale rose	15.4811(7)	161	440[c]
δ-KHo_3F_{10},xH_2O	Pale yellow	15.5526(9)	190	414[c]
δ-KY_3F_{10},xH_2O	White	15.4917(7)	188	445[c]
δ-$RbLu_3F_{10},xH_2O$	White	15.3151(11)	160	468
δ-$RbYb_3F_{10},xH_2O$	White	15.3758(7)	165	462
δ-$RbTm_3F_{10},xH_2O$	White	15.4631(6)	165	472
δ-$RbEr_3F_{10},xH_2O$	Pale rose	15.5353(5)	150	475
δ-RbY_3F_{10},xH_2O	White	15.5761(4)	160	433
δ-$CsLu_3F_{10},xH_2O$	White	15.2730(8)	110	335
δ-$CsYb_3F_{10},xH_2O$	White	15.3312(8)	120	435
δ-$CsTm_3F_{10},xH_2O$	White	15.4110(14)	150	430
δ-$CsEr_3F_{10},xH_2O$	Pale rose	15.4714(26)	110	370
δ-CsY_3F_{10},xH_2O	White	15.5261(20)	117	415
δ-$(NH_4)Lu_3F_{10},xH_2O$	White	15.2910(5)	160	455
δ-$(NH_4)Yb_3F_{10},xH_2O$	White	15.3531(6)	150	335
δ-$(NH_4)Tm_3F_{10},xH_2O$	White	15.4198(5)	100	390
δ-$(NH_4)Er_3F_{10},xH_2O$	Pale rose	15.5254(8)	160	300
δ-$(NH_4)Y_3F_{10},xH_2O$	White	15.5627(8)	160	250
δ-$Li_{0.5}(H_3O)_{0.5}Yb_3F_{10},xH_2O$[d]	White	15.3240(10)	153	313
δ-$Na_{0.8}(H_3O)_{0.2}Yb_3F_{10},xH_2O$[d]	White	15.2957(10)	170	430

[a]Temperature corresponding to the departure of zeolitic water. [b]Decomposition temperature. [c]Structural transition δ→α. [d]Obtained by cationic exchange.

2 Characterization

The sample purity was checked by X-ray diffraction on a $\theta/2\theta$ Siemens D500 diffractometer operated at room temperature. The cell parameters were refined with the "pattern matching" mode of the Fullprof program.[6] We must keep in mind that the zeolitic behavior of these phases makes it difficult to compare cell parameters between the compounds. Indeed, as we will see in Section 4, the absorption of water is very fast and naturally depends on the moisture content of the atmosphere. Nevertheless, and as expected for the same A^+ ion, the overall lattice volume changes linearly with the ionic size of the rare earth[7] in good agreement with the lanthanide contraction except for yttrium which is not a lanthanide (see Fig. 3 for $A^+=K^+$). This behaviour has been systematically observed for all the A^+ cations.

In order to determine the cationic exchange ratio, quantitative analyses by atomic emission spectrometry (AES) have been carried out on the Li^+ and Na^+ exchanged phases. This study has been performed on compounds obtained from δ-$(H_3O)Yb_3F_{10},xH_2O$ and δ-KYb_3F_{10},xH_2O to determine if the nature of the A^+ ion in the starting phase could influence the cationic exchange. For the compounds obtained from δ-KYb_3F_{10},xH_2O, AES analysis allowed us to determine the quantity of lithium (or sodium) and the remaining potassium. The results show that the cationic exchange ratio is never complete leading to the following formula: δ-$Li_{0.38}K_{0.62}Yb_3F_{10},xH_2O$ and δ-$Na_{0.76}K_{0.24}Yb_3F_{10},xH_2O$. This

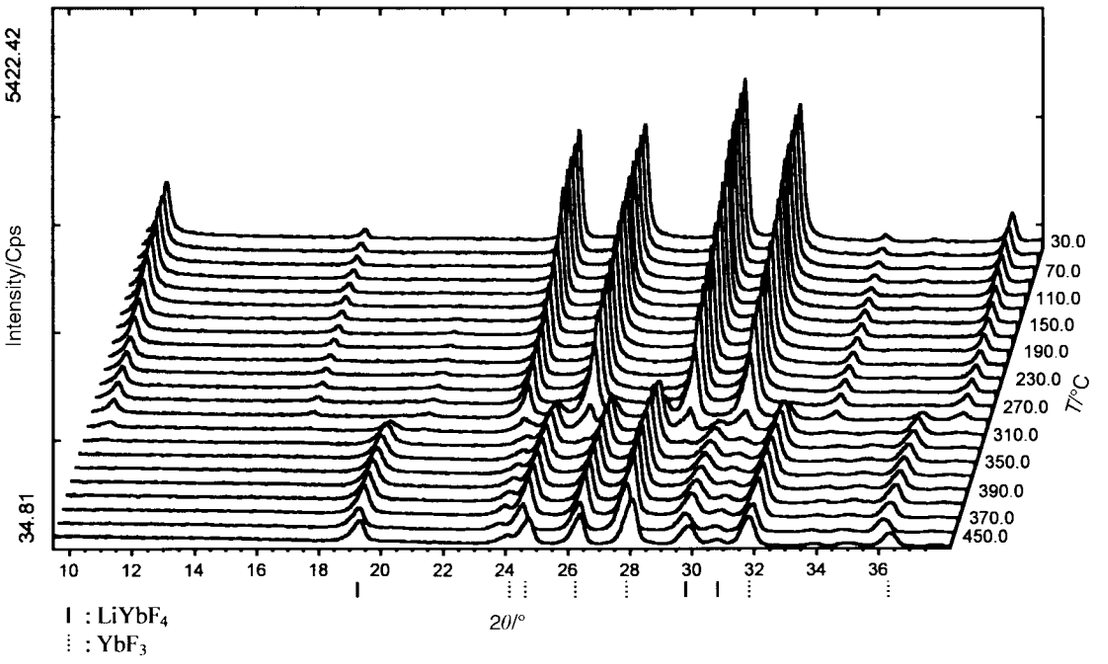

Fig. 4 X-Ray thermodiffractogram of δ-$(Li)_{0.5}(H_3O)_{0.5}Yb_3F_{10},xH_2O$.

can be confirmed by X-ray diffraction since the (222) peak is sensitive to the nature of the A^+ cation. This peak appears on the δ-KYb_3F_{10},xH_2O diagram and still remains slightly visible after cationic exchange.

AES analysis was then used to determine the exchange rate $Li^+ \leftrightarrow H_3O^+$ (or $Na^+ \leftrightarrow H_3O^+$). After five successive exchanges, the analysis led to the formula δ-$Li_{0.50}(H_3O)_{0.50}Yb_3F_{10},xH_2O$ and δ-$Na_{0.80}(H_3O)_{0.20}Yb_3F_{10},xH_2O$.

These partially exchanged phases could in fact be a mixture of two phases with close cell parameters: δ-$(H_3O)Yb_3F_{10},xH_2O$ and δ-$LiYb_3F_{10},xH_2O$. This was suggested by a careful examination of the X-ray thermodiffractogram realised on δ-$Li_{0.50}(H_3O)_{0.50}Yb_3F_{10},xH_2O$ (see Fig. 4). The data collection was performed under a helium flow on a Siemens D5000 (θ/θ configuration) equipped with a PSD (Elphyse) and a high temperature attachment Anton Parr HTK10 using Cu radiation and with the following conditions: step = 0.03° (2θ), collection time = 28 minutes for $5° < 2\theta < 90°$, heating rate = 5 °C s^{-1}, ΔT = 20 °C and a delay of 300 s before each scan. At T = 270 °C, only the lines relative to YbF_3 begin to appear. This temperature corresponds to the decomposition temperature of dehydrated δ-$(H_3O)Yb_3F_{10}$ determined by DTA measurements. Then, above T = 290 °C, $LiYbF_4$ becomes visible in relation to the decomposition of the dehydrated "δ-$LiYb_3F_{10}$" compound.

3 Thermal characterization

DTA experiments (T.A. Instruments SDT 2960) allowed us to determine the thermal characteristics of these phases (see Table 1). Except for $A^+ = H_3O^+$, all the compounds present a similar behaviour (Fig. 5a) with a first large endothermic peak associated with an important loss of matter. It corresponds in fact to a loss of water without a modification of the crystalline network. The second peak, exothermic, is due to the decomposition of the starting phase except for the case with $A^+ = K^+$. Indeed, for these compounds, this peak is correlated to the irreversible transition from anhydrous δ-KLn_3F_{10} to the α-KLn_3F_{10} form (Fig. 5b). Considering the exothermic peak as indicating the thermal stability, it appears that the series with $A^+ = Rb^+$ is the most stable (see Table 1). For the series δ-$(H_3O)Ln_3F_{10},xH_2O$, the DTA–TGA diagram clearly exhibits three thermal phenomena. The first two peaks (Fig. 5c), both endothermic, are associated with the departure of water:

(1) Zeolitic and adsorbed water : δ-$(H_3O)Ln_3F_{10},xH_2O \rightarrow$ δ-$(H_3O)Ln_3F_{10} + xH_2O$

(2) Elimination of H_2O from H_3O^+: δ-$(H_3O)Ln_3F_{10} \rightarrow$ "δ-$(H)Ln_3F_{10}$" + H_2O

The third peak, exothermic, corresponds to the decomposition of δ-$(H)Ln_3F_{10}$ into HF and $3LnF_3$.

For $A = H_3O^+$, the thermal stability of the δ-phases is related to the rare earth size: the most stable compound is observed for the smaller lanthanide ion. For the other phases the correlation is not obvious.

4 Zeolitic behaviour

As already mentioned, the peculiar structure, based on the association of LnF_8 square antiprisms, involves a zeolitic behaviour for all the δ-ALn_3F_{10},xH_2O phases. Six LnF_8 antiprisms are connected together to build up a $[Ln_6F_{32}]^{14-}$ structural unit with an octahedron like geometry (see Fig. 6a). This unit is denoted $UOA_{[8]}$; the index [8] indicates the number of anions which constitute the central cavity (cubic in this case). These $UOA_{[8]}$, connected by vertices, describe a diamond-type stacking leading to a three-dimensional $[Ln_6F_{20}]^{2-}$ network. This association of octahedral units creates cavities linked together by tunnels as can be seen on Fig. 6b. The cavity, centred on the 8b site (Fig. 6c), is delimited by $28F^-$ and its free diameter is about 6 Å which corresponds to a free volume of 110 $Å^3$. The water molecules are located in the cavities (site 48f) and can move through the tunnels which connect the cavities. The pore size, corresponding to the hexagonal window of a cavity, has a free diameter of about 2.88 Å.

Several experiments have been performed to provide evidence for the zeolitic compartment. At first, X-ray thermodiffractometry was performed under a helium gas flow (Siemens D5000, step = 0.03° (2θ), collection time = 38 minutes for $7° < 2\theta < 120°$, heating rate = 5 °C s^{-1}, ΔT = 20 °C, delay before each scan = 300 s). The measurements allowed us to follow the evolution of the compound during heating. The X-ray thermodiffractogram realised with δ-KYb_3F_{10},xH_2O from room temperature to 450 °C is presented in Fig. 7. No decomposition of the product is observed below T = 390 °C. We only note a shift of the peaks, due to cell parameter variation. Above 390 °C, new lines corresponding to the α-KYb_3F_{10}

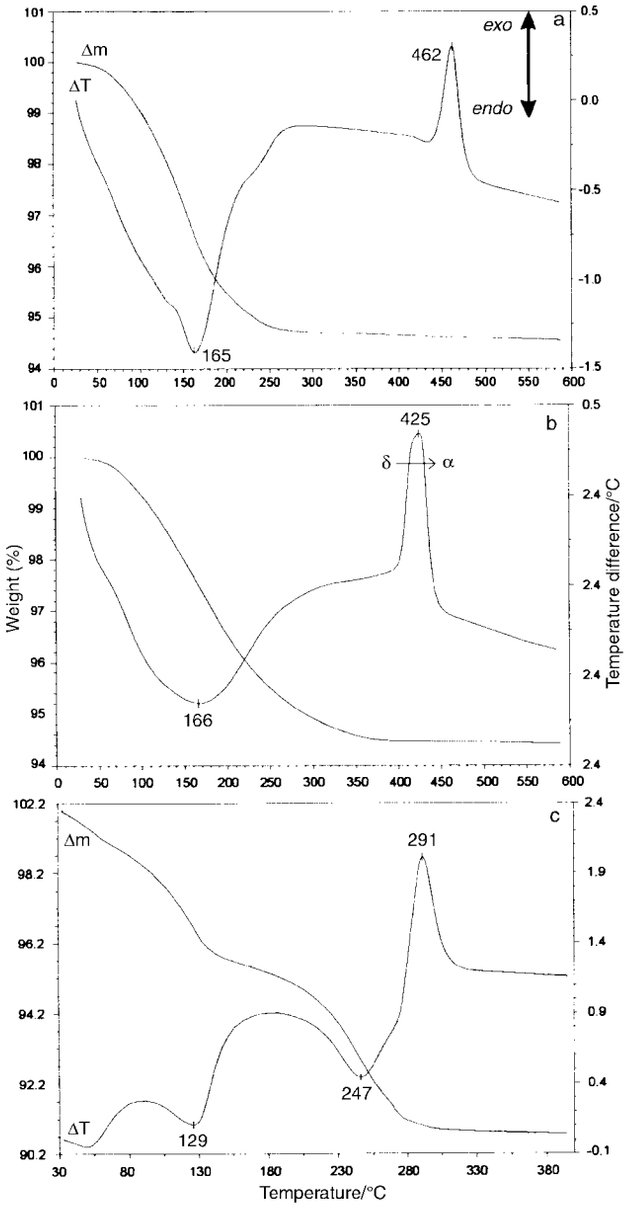

Fig. 5 DTA–TGA curves for δ-$RbYb_3F_{10},xH_2O$ (a), δ-KYb_3F_{10},xH_2O (b) and δ-$(H_3O)Yb_3F_{10},H_2O$ (c).

phase begin to appear. The pattern matching mode of the Fullprof program[6] was used to refine the cubic cell parameter for each temperature. Fig. 8a shows the cell parameter variation of δ-KYb_3F_{10},xH_2O during heating. As the temperature increases, the decrease of the cell parameter from $a=15.292$ Å to 15.239 Å corresponds to the loss of zeolitic water. Then the cell parameter starts to increase for $T=190$ °C which is due to the thermal expansion of the crystalline network. In good agreement with the DTG–DTA measurements, for $T>390$ °C, no more variation is observed and the cell parameter remains constant, connected to the α form's appearance.

The rehydration phenomenon was studied using a new sample heated under vacuum up to 380 °C for one hour and then cooled down to room temperature. At this point the refined cell parameter is 15.230(2) Å. Then the high temperature attachment was first filled with helium gas; a new measurement of the cell parameter showed an increase up to 15.260(2) Å, probably due to traces of water inside the gas pipe. Finally, the X-ray chamber was opened to air and the X-ray data were collected every two minutes ($7°<2\theta<120°$). The evolution of the refined cell parameter is shown in Fig. 8b.

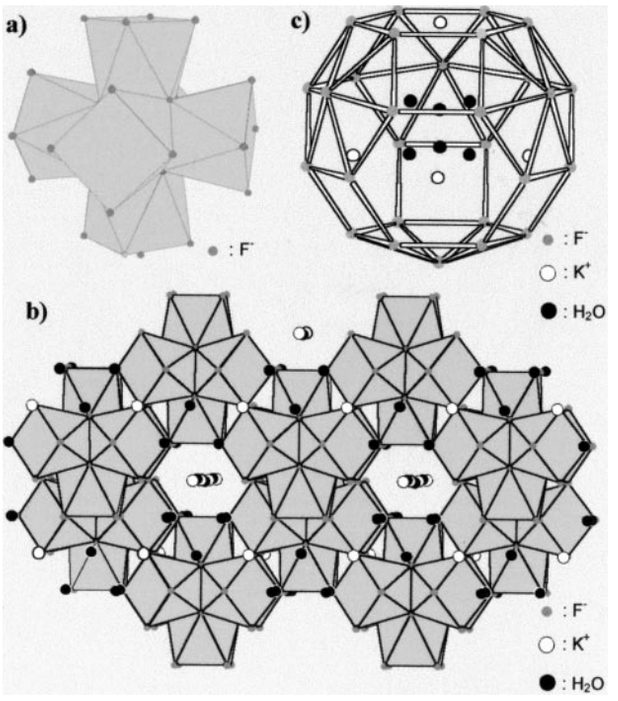

Fig. 6 $UOA_{[8]}$ or $[Ln_6F_{32}]^{14-}$ structural unit (a); view of the structure of δ-ALn_3F_{10},xH_2O along [110] showing the tunnels (b); cage built up from the association of 10 $UOA_{[8]}$ (c).

From the observed increase (15.260(2) Å to 15.298(2) Å) we deduce that water reabsorption is very fast (assuming that the cell parameter is proportional to water content, 85% of the water reabsorption measured after contact with air was obtained in only 12 minutes).

The zeolitic character was also studied by DTA–TGA experiments. With a well defined temperature program we followed the weight variation during two cycles of absorption–desorption (Fig. 9). The compound was first heated at 300 °C under an argon flow for two hours in order to enable the departure of water (−5.82%). Then, it was cooled under an air flow and left for two hours. During this step and as we can see in Fig. 9, the weight increase (+4.18%), not far from the saturation, corresponds to reabsorbed water. If the heated compound is assumed to be anhydrous, the formulation at the end of the cooling is δ-$KYb_3F_{10},1.8H_2O$ and must be close to the equilibrium formulation. The same calculation is used to determine the initial water content before heating. It leads to δ-$KYb_3F_{10},2.26H_2O$. The difference between both water contents (initial and zeolitic), systematically observed with all the compounds δ-ALn_3F_{10},xH_2O, may correspond to adsorbed water.

The same study performed on δ-$(H_3O)Yb_3F_{10},xH_2O$ showed that this compound, after two cycles of dehydration–hydration, systematically reabsorbs a mass corresponding to one mole of water.

5 Magnetism

Susceptibility measurements were performed in the temperature range 4.2 K–300 K using a Faraday method ($H=9$ kGauss). The thermal variation of the inverse susceptibility is given in Fig. 10 for δ-KLn_3F_{10},xH_2O compounds. For $Ln^{3+}=Tm^{3+}$, Ho^{3+} and Er^{3+}, a Curie–Weiss law is observed nearly on the totality of the temperature range and the calculated effective moments per Ln ion are close to the expected values (Table 2). Below 50 K, a deviation from linearity is observed for KYb_3F_{10},xH_2O, probably due to the zero-field splitting of the Yb^{3+} multiplet induced by the crystal

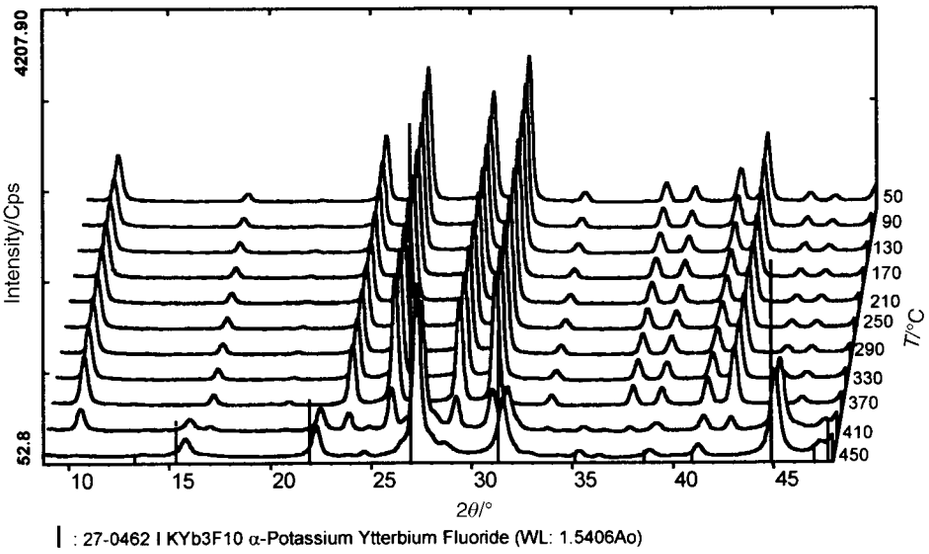

Fig. 7 X-Ray thermodiffractogram of δ-KYb_3F_{10},xH_2O.

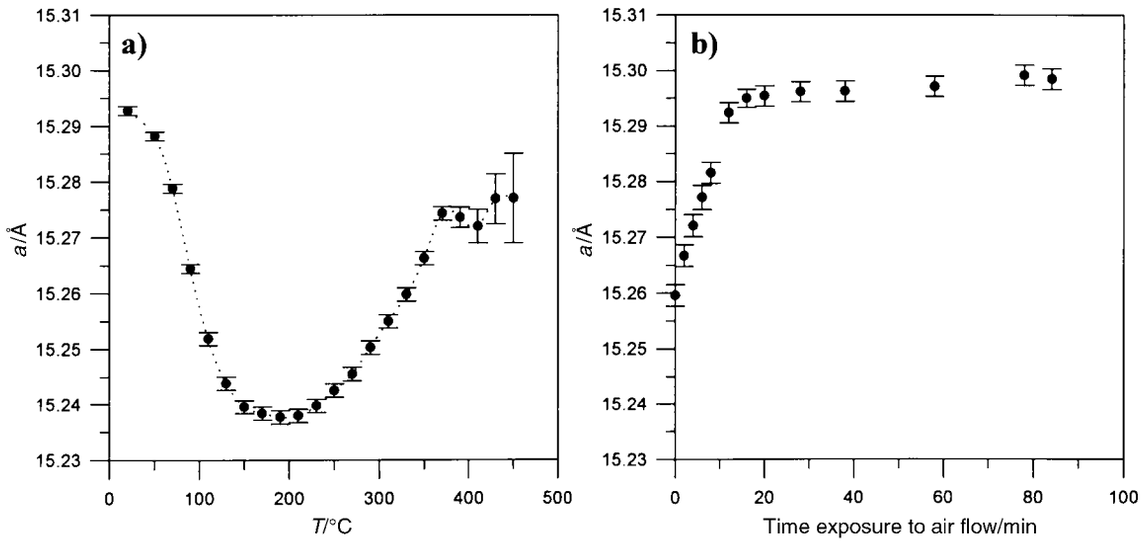

Fig. 8 Cell parameter evolution of δ-KYb_3F_{10},xH_2O *versus* the temperature (a) and *versus* exposure time to air (b).

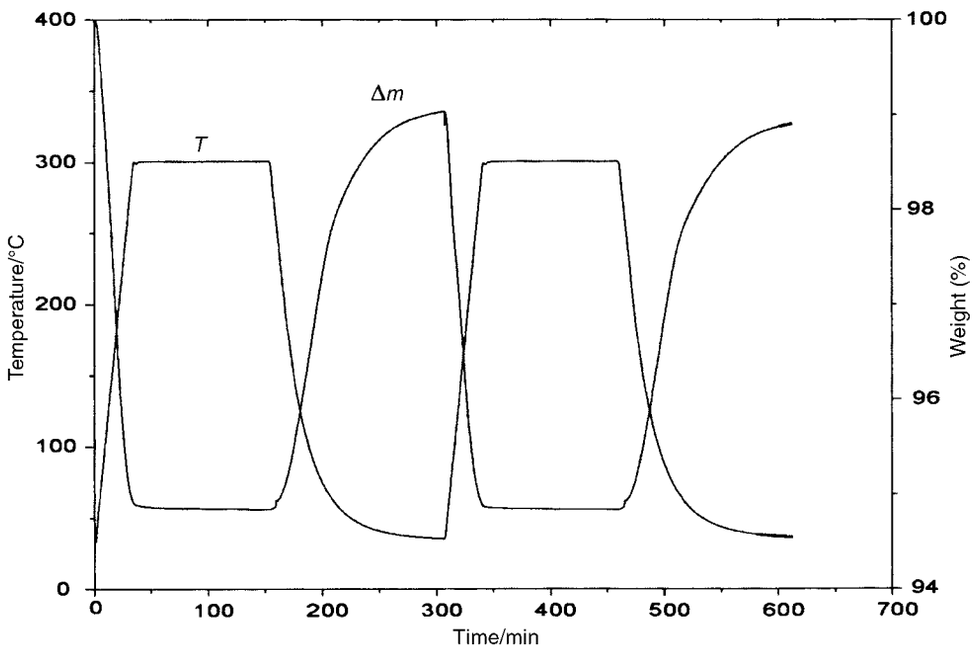

Fig. 9 TGA curves for δ-KYb_3F_{10},xH_2O.

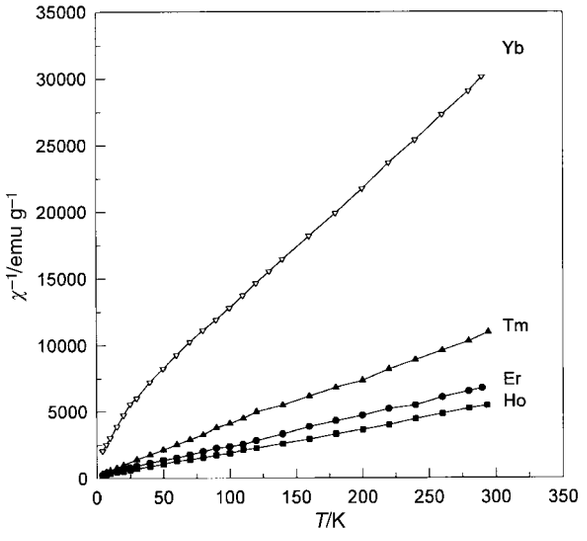

Fig. 10 $\chi^{-1}=f(T)$ curve for δ-KLn_3F_{10},xH_2O.

Table 2 Magnetic data of δ-KLn_3F_{10},xH_2O

Compound	θ_p/K	C_M	$\mu_{eff}{}^a/\mu_B$	$\mu_{theo}{}^a/\mu_B$
δ-KYb_3F_{10},xH_2O	−48	8.21	4.68	4.54
δ-KTm_3F_{10},xH_2O	−7	20.93	7.47	7.56
δ-KEr_3F_{10},xH_2O	−4	32.71	9.34	9.59
δ-KHo_3F_{10},xH_2O	−2	40.67	10.41	10.60

[a]Magnetic moment per one lanthanide ion.

field. As expected, no influence of the ion A^+ on the magnetic characteristics has been noticed.

The magnetization has been measured for δ-KHo_3F_{10},xH_2O at $T=2.3$ K. An observed magnetic moment of 5.38 μ_B at $H=40$ kGauss, lower than the expected gJ value (10 μ_B), indicates that the saturation is not reached.

B The γ-$ThEr_2F_{10},H_2O$ family

As previously seen, the structure of the δ-ALn_3F_{10},xH_2O compounds can be described by a stacking of $UOA_{[8]}$ which leads to a negatively charged network $[Ln_6F_{20}]^{2-}$. In this network, the cation A^+ located at the centre of the four open faces of the cage may obstruct the departure of the H_2O molecules situated inside this cage (Fig. 6c). Then, in order to improve the zeolitic character, we tried to create a neutral framework, which can be obtained by substituting the Ln^{3+} and A^+ cation by a tetravalent cation such as Th^{4+}. According to the following scheme: "$A^+ + 3Ln^{3+} \rightarrow Th^{4+} + 2Ln^{3+}$", compounds with formula δ-$ThLn_2F_{10},xH_2O$ are expected.

1 Synthesis

A "chimie douce" technique, very similar to that described in A-1, was used. All syntheses had to be performed in the pH range 4–6. In a first step, a mixture of thorium and lanthanide salts (either nitrates or chlorides) were dissolved in hot water ($[Th^{4+}]=0.035$ M (slight excess); $[Ln^{3+}]=0.061$ M). The resulting solution was added to a 0.48 M solution of NH_4F under stirring and maintained at 75 °C for 30 minutes. After filtration, washing and drying, the final product was obtained in the form of a fine powder with no single crystal included. Such a synthesis was achieved for $Ln^{3+}=Dy^{3+}$, Er^{3+} and Yb^{3+}.

2 Characterization

As expected, a chemical analysis performed by inductively coupled plasma (ICP) gives a molar ratio [Ln]/[Th] close to 2.

The infrared spectroscopy (spectra monitored between 500 and 4000 cm^{-1}) confirms the presence of water molecules in the compound. At 1630 cm^{-1} a band is observed, characteristic of the δ_{H2O} vibration frequency of H_2O and a broad peak is visible at 3300–3600 cm^{-1} which corresponds to ν_{OH}.

The coupled thermogravimetric and thermal analysis data collected up to 600 °C are shown Fig. 11. The loss of matter is due to water departure (adsorbed and zeolitic). At $T=480$ °C, an exothermic peak becomes visible and is attributed to the decomposition of the anhydrous product $ThEr_2F_{10}$ into ThF_4 and ErF_3. Assuming the compound is perfectly anhydrous before the decomposition, the initial water content may be estimated as 5.2 moles per formula unit.

The X-ray pattern is different from those characteristic of the δ-phases but is similar to that of the γ-KYb_3F_{10} phase. The

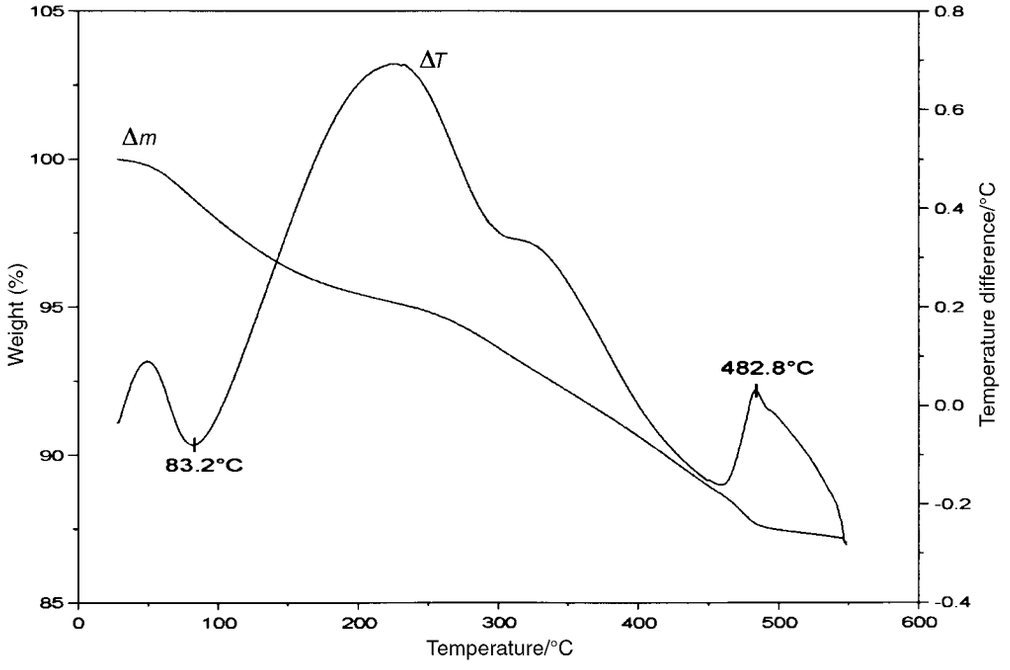

Fig. 11 DTA–TGA curves for γ-$ThEr_2F_{10},H_2O$.

Table 3 Conditions of powder data recording (300 K) and refinement for γ-$ThEr_2F_{10},xH_2O$

Angular range/°(2θ)	7–130		
Step/°(2θ)	0.02		
Time per step/s	30		
Receiving slits/°	0.2		
Refinement program	Fullprof		
Space group	$Fm\bar{3}m$ (no. 225)		
Cell parameters/Å	$a=11.739(1)$		
Volume/Å^3, Z	137.80, 8		
Zero point/°(2θ)	0.0496		
Background	Selected by hand		
Number of reflections	206		
Peak shape	pseudo-Voigt		
FWHM parameters	$u=0.165(7)$	$v=-0.098(6)$	$w=0.048(1)$
Asymmetry parameters	0.06998		
Number of parameters	15		
Conventional reliability factors	$R_p=10.8\%$	$R_{wp}=10.8\%$	$\chi^2=12.3$
	$R_B=5.86\%$	$R_f=4.19\%$	

symmetry remains cubic with a unit cell parameter close to 11.7 Å.

3 Structure determination

The structure of $ThEr_2F_{10},xH_2O$ was determined in the space group $Fm\bar{3}m$ ($Z=8$) assuming that it was isotypic with the γ-KYb_3F_{10} type. The X-ray powder diffractogram was collected on a $\theta/2\theta$ Siemens D500 diffractometer at room temperature. Heavy atoms (1/3 Th^{4+} + 2/3 Er^{3+}) were located in a 24e site (0.2425 0 0). After refinement of the atomic position and thermal motion, the difference Fourier map, calculated from SHELXS-86,[9] showed several peaks. According to the bound distances, the fluorine atoms were placed in a 32f position (0.116 0.116 0.116) for F1 and in a 48i position (0.5 0.334 0.334) for F2. At this stage, an electron density peak situated on a 8c position (0.25 0.25 0.25) was still observed. This peak was explained by water molecules. After refinement of parameters, the conventional values are: $R_p=10.8\%$, $R_{wp}=10.8\%$, $\chi^2=12.3$, $R_B=5.86\%$, $R_f=4.19\%$. The composition was then: γ-$ThEr_2F_{10},H_2O$. The conditions of data collection and refinement are reported in Table 3, the atomic and thermal motions parameters in Table 4 and selected bond lengths in Table 5. The observed and calculated patterns are presented in Fig. 12.

4 Zeolitic behaviour

The γ structure has been described using a CCP stacking of $UOA_{[8]}$.[8] The units $UOA_{[8]}$ are linked by vertices and are centred on the 4a (0 0 0) position. The formulation of the three-dimensional network still remains $[Ln_6F_{20}]^{2-}$ or in our case $[Th_2Ln_4F_{20}]^{2-}$ with $Z=4$. The water molecules are located on the 8c position (¼ ¼ ¼) which corresponds to the centre of a cavity delimited by $16F^-$ (free diameter about 3.6 Å which means a free volume close to 25 Å^3). All the cavities, directly connected together *via* F_2–F_2 edges ($d_{F2-F2}=2.79$ Å), build three-dimensional channels where water molecules can move (Fig. 13). These compounds exhibit a zeolitic behaviour, which has been studied by TGA and X-ray thermodiffractometry.

Fig. 14 shows the weight variation observed during three cycles of dehydration–hydration. The compound is first heated at 280 °C under argon and then cooled under an air flow. From the TGA curve, this temperature may not be high enough to totally dehydrate the compound. However, the same experiment realised at 300 °C, showed a partial decomposition of the phase in ThF_4 and ErF_3 due to kinetic effects. During the first step of heating, a weight loss (7.1%) was observed corresponding to a loss of water. As we saw previously for the δ compounds, this initial water content is never fully reabsorbed since the successive cooling and heating lead to a mass variation close to 2.3%. Even if we are not in equilibrium conditions, the recurrent mass variation corresponds to the reabsorption of about one water molecule per formula unit in agreement with the results of the structural study. The mass difference (7.1%–2.3%) is due to adsorbed water. At the end of each dehydration, the mass obtained slightly decreases as the number of cycles increases. This suggests that the temperature (280 °C) may be too low to enable complete water departure after just one cycle.

These observations have been also verified by X-ray thermodiffractometry, which allowed us to follow the cell parameter evolution during dehydration (Fig. 15). At first, no cell parameter change was observed until $T>120$ °C. An important decrease then became visible corresponding to the departure of the zeolitic water and the shape of the resulting $a=f(T)$ curve looks like the TGA curve.

Table 4 Atomic parameters and B_{iso} temperature factors (Å^2) for γ-$ThEr_2F_{10},H_2O$

Atom	Site	x	y	z	B_{iso}
Th/Er	24e	0.2425(4)	0	0	1.28(1)
F1	32f	0.1157(4)	0.1157(4)	0.1157(4)	1.14(1)
F2	48i	0.5	0.3339(5)	0.3339(5)	1.14(1)
O (H_2O)	8c	0.25	0.25	0.25	2.32(2)

Table 5 Main distances (Å) in γ-$ThEr_2F_{10},H_2O$

F–F distances in the square antiprism	(Er^{3+}, Th^{4+}) polyhedron [8]	Zeolitic water
$3\times F_1$–$F_1=2.71(1)$	$4\times$(Er,Th)–$F_1=2.43(1)$	$4\times(H_2O)$–$F_1=2.72(1)$
$4\times F_1$–$F_2=2.95(1)$	$4\times$(Er,Th)–$F_2=2.22(1)$	$12\times(H_2O)$–$F_2=3.24(1)$
$4\times F_2$–$F_2=2.75(1)$		
$1\times F_2$–$F_2=2.78(1)$		

C Discussion and conclusion

During the dehydration–hydration process, we noted, for δ-KYb_3F_{10},xH_2O, a reproducible gain of water corresponding to 1.8 molecules. This water content corresponds for the 48f site, to an occupation factor of 3/5 and means that the δ-phase is able to accept more than two water molecules per cavity in agreement with its large free volume (110 Å^3). For γ-$ThEr_2F_{10},H_2O$, the additional water content observed during thermal experiments can be explained by the presence of

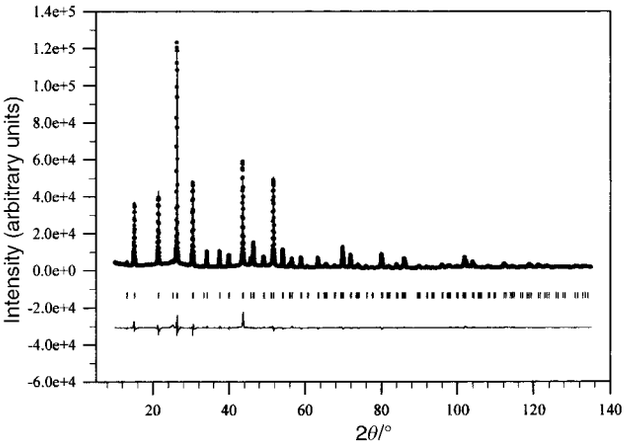

Fig. 12 Observed (—) and calculated (···) X-ray patterns of γ-$ThEr_2F_{10},H_2O$. The difference pattern is shown below at the same scale (vertical bars are related to the calculated Bragg reflection's position).

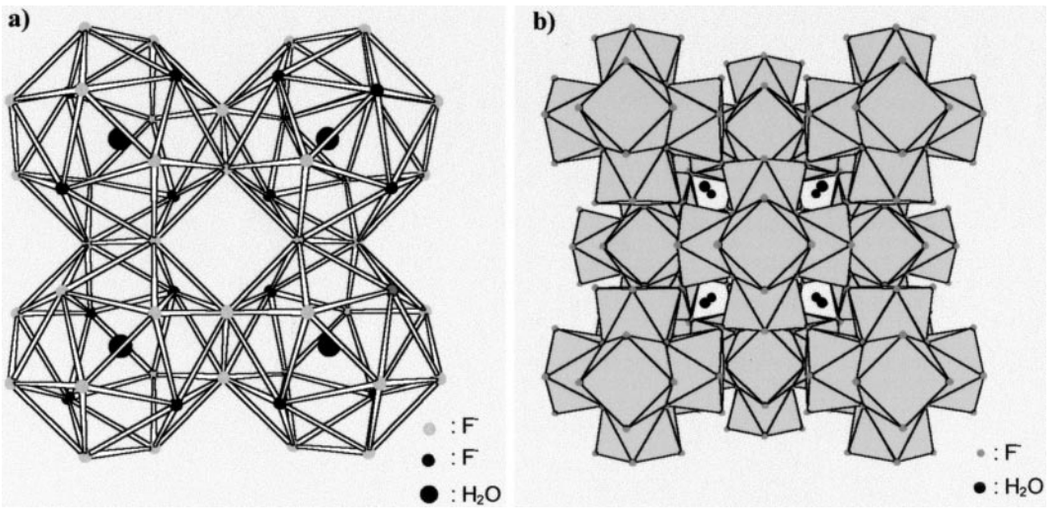

Fig. 13 Cages containing H_2O connected together *via* F_2–F_2 edges (a); structure of γ-$ThEr_2F_{10},H_2O$ viewed along [0 0 1] showing tunnels (b).

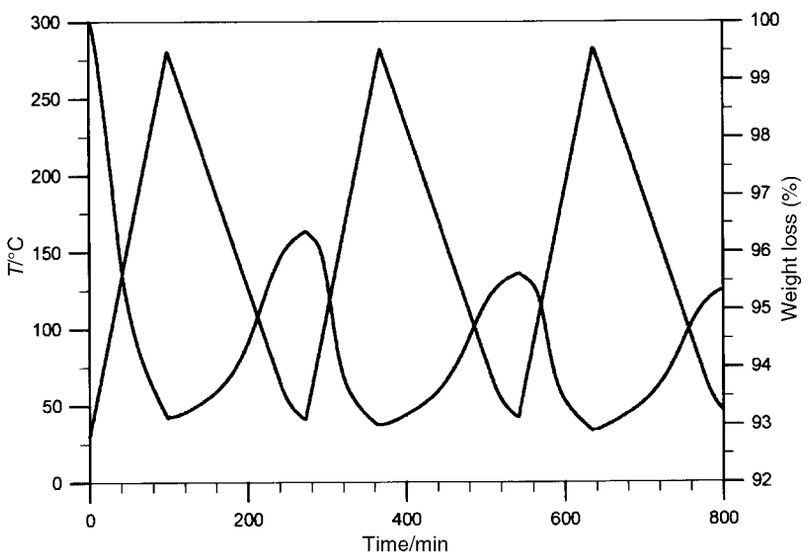

Fig. 14 TGA experiment under an air flow for γ-$ThEr_2F_{10},H_2O$.

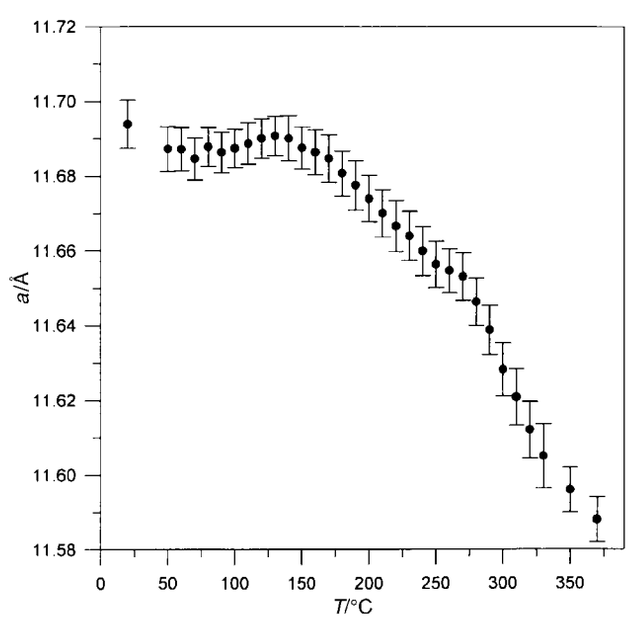

Fig. 15 Cell parameter variation of γ-$ThEr_2F_{10},H_2O$ *versus* the temperature.

adsorbed water at the grain surface and depends on the moisture content of the atmosphere.

Concerning the desorption–absorption of the zeolitic water, the δ-phase seems to proceed faster than γ-$ThEr_2F_{10},H_2O$. Nevertheless we are not able to explain this observation because for the δ compounds the A cations prevent the departure of water if they don't move away from the pseudo-hexagonal gate of the cavity (16c site). On the contrary, for the γ-phase, no cation prevents the water motion through the cavities; only a steric constraint due to small triangular windows of fluorine atoms (mean F–F distance close to 2.8 Å) may slow down the water displacement and consequently reduce the rate of desorption (or absorption). This can explain the difficulty in completely dehydrating the γ phase during the cycles of dehydration–hydration.

In conclusion, the present study allowed us to fully characterise the δ-ALn_3F_{10},xH_2O family. Substitutions of the alkaline and lanthanide cations of the original phase δ-$(H_3O)Yb_3F_{10},H_2O$ have been performed. The synthesis temperature of these phases, obtained using a "chimie douce" technique, depends on the ionic radius of the rare earth. Their structure confers upon them a zeolitic behavior as revealed by TGA and X-ray thermodiffractometry measurements. A new zeolitic phase corresponding to the formula γ-$ThLn_2F_{10},H_2O$ has also been discovered. The thermal stability of these phases

extends in the range 250–480 °C; however the zeolitic water capacity (about 2–4% in mass) remains low.

Acknowledgements

The authors gratefully acknowledge Dr Pena (University of Rennes I) for magnetization measurements.

References

1 M. Labeau, S. Aléonard, A. Védrine, R. Boutonnet and J. C. Cousseins, *Mater. Res. Bull.*, 1974, **9**, 615.
2 S. Aléonard, J. C. Guittel, Y. Le Fur and M. T. Roux, *Acta Crystallogr., Sect. B*, 1976, **32**, 3227.
3 R. Boutonnet, PhD Thesis, University of Clermont Ferrand, 1974.
4 A. Arbus, M. T. Fournier, B. Picaud, G. Boulon and A. Védrine, *J. Solid State Chem.*, 1980, **31**, 11.
5 J. J. Maguer, M. P. Crosnier-Lopez and G. Courbion, *J. Solid State Chem.*, 1997, **128**, 42.
6 J. Rodriguez-Carvajal, *Fullprof 98*, version 02, 1998.
7 R. D. Shannon, *Acta Crystallogr., Sect. A*, 1976, **32**, 751.
8 J. J. Maguer and G. Courbion, *J. Solid State Chem.*, 1997, **128**, 52.
9 G. M. Sheldrick, A Program for Crystal Structure Determination, University of Göttingen, Germany, 1986.